Beam-induced wakefield observation in *X*-band choke-mode cavities

Hao Zha,[1,2,4] Chunguang Jing,[2,3,*] Jiaqi Qiu,[2,3] Eric E. Wisniewski,[2] Manoel Conde,[2] John G. Power,[2] Darrell S. Doran,[2] Wanming Liu,[2] Jiaru Shi,[1,4,†] Chen Li,[1,2] Wei Gai,[1,2] and Huaibi Chen[1]

[1]*Department of Engineering Physics, Tsinghua University, Beijing 100086, China*
[2]*Argonne National Laboratory, Argonne, Illinois 60439, USA*
[3]*Euclid Tech labs LLC, Solon, Ohio 44139, USA*
[4]*CERN, European Organization for Nuclear Research, Geneva 1211, Switzerland*
(Received 11 February 2016; published 1 August 2016)

The *X*-band choke-mode structure is currently being studied as an alternative design for the accelerating structure of the compact linear collider (CLIC) main linac. The geometry of the choke-mode structure is designed to ensure the strong suppression of the beam-induced long-range transverse wakefield and therefore maintain the stability and quality of the beam in the CLIC main linac. Experiments conducted at the Argonne Wakefield Accelerator Facility are presented in this study to verify the design of the wakefield suppressor. The beam-induced radio frequency (rf) signals in a three-cell choke-mode structure were measured, and measured results show good agreement with the simulation results. The measured results also show strong damping in high-order dipolar modes with a quality factor Q of 10 to 20. The difference between the frequencies of the first and second dipole modes is about 3 GHz, which validates the special design of the cancelling dipole modes at the time of the succeeding bunch (0.5 ns).

DOI: 10.1103/PhysRevAccelBeams.19.081001

I. INTRODUCTION

As the dimensions of accelerating structures become smaller or beam intensities higher, the transverse wakefields driven by the beam become quite large with even a slight misalignment of the beam from the geometric axis. These deflection modes can cause interbunch beam breakup and intrabunch head-tail instabilities along the beam path [1,2]. There are strict requirements of transverse wakefield damping for these high-frequency band room-temperature accelerator structures with multibunch operation [3–7].The choke-mode accelerating structure has been studied for two decades [8–10]. As shown in Fig. 1, its geometry is designed to use rf loads to absorb the beam-induced high-order-mode (HOM) wakefield. The fundamental working frequency is fully reflected by the choke-structure to prevent the degradation of the Q-factor. The choke-mode design involves potentially lower manufacturing cost and lower surface magnetic field than other accelerating structures with HOM suppression; thus, it is very attractive for future particle accelerator projects. The *X*-band choke-mode structure is currently being studied as an alternative design for the accelerating structure of the compact linear collider (CLIC) main linac [11,12].

CLIC is one of the candidate project for a future lepton collider [13]. In its design scheme, electron and positron beams are accelerated to the energy of 1.5 TeV in two identical 21-km-long linacs which are mainly composed of high gradient normal conducting *X*-band structures. Such a long, high frequency band accelerating structure results in strong long-range transverse wakefield induced by the beams, which may cause multibunch instability. The

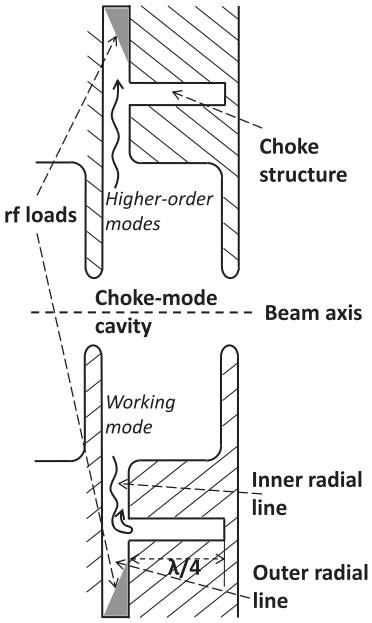

FIG. 1. Choke-mode accelerating structures.

*jingchg@anl.gov
†shij@mail.tsinghua.edu.cn

baseline design of the CLIC main linac accelerating structure employs a waveguide damping scheme to provide strong and broadband suppression of all the HOMs [14]. Alternative designs include the choke-mode structure and damped-detuned structure (DDS) [15], which are also currently being studied.

The rf design of the CLIC choke-mode structure is established and named "CLIC-CDS-C" [12]. Compared to the first version of CLIC choke-mode structure design "CDS-A" [11], this design version improved the choke geometry to enhance the suppression of all major dipolar modes from 15 GHz to 40 GHz, of which the Q factors are reduced to the level of 10. In addition, the geometry is designed to sustain 3 GHz frequency difference between the first and the second dipolar modes to reduce the wakefield kick by canceling the two dipolar modes at the time of the next bunch (0.5 ns). The geometry of structure tested in this experiment was based on the middle cell of the CDS-C structure design. Figure 2 shows the transverse wakefield spectrum in the middle cell (The spectrum of the full CDS-C structure can be found in Ref. [12], Fig. 16).

In this study, we present a wakefield measurement experiment of an X-band choke-mode structure at the Argonne Wakefield Accelerator (AWA) Facility [16]. An electron bunch with a charge of 5 nC was injected to the test setup to excite the wakefields in the structure under test. The wakefield signal was picked up by rf probes inside the outer radial line of choke-mode cells and recorded by oscilloscope. The structure under test is transversely movable; thus, the monopole or dipole modes can be discriminated from the signal scanning on the transverse offset. Similar experiments were conducted for PBG cavities [17–19], where the Q factors of the HOMs were measured at the level of 50–100. However, the major dipolar modes in the CLIC choke-mode structure are heavily damped with Q factors at the level of 10–20 resulting in significant challenges in identification and analysis of dipole mode signals from the measured signal spectrum (i.e. very low signal to noise ratio).

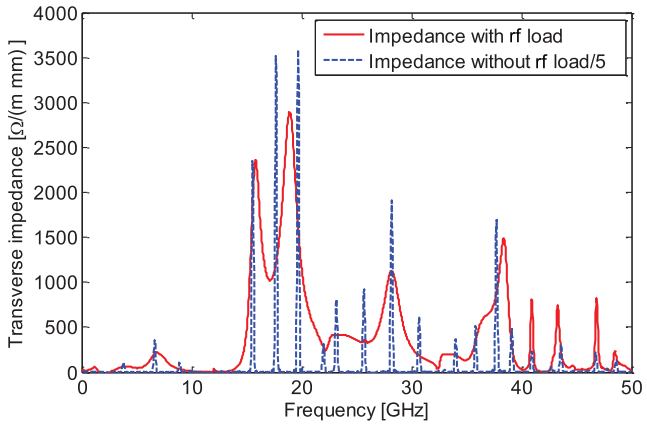

FIG. 2. Transverse wakefield spectrum in the middle cell of the CDS-C design.

The objective of the experiment is to verify the suppression feature of HOMs in CLIC choke-mode cavities. This is realized by the evaluation of the very low Q values in addition to the frequency determination of the dipole modes. Aside from the choke-mode structure, there are other kinds of heavily damped structures, such as the waveguide damped structure and iris slotted damped structure [20]. These structure designs have drawn much interest in the study of high-gradient normal conducting accelerating structures. The technique used to measure and analyze the wakefield signal developed in this experiment can also be useful in similar experiments on all other heavily damped structures.

Several long-range wakefield experiments have been conducted using a second particle beam to directly measure the value of wakefield kick [5,21–23]. However, these experiments can only be performed in facilities with two independent beam lines, such as the FACET facility at SLAC National Accelerator Laboratory [24]. (The AWA facility also has two independent beam lines installed. However, only one beam line was available at the time of this experiment.)

II. EXPERIMENT SETUP

Figure 3 shows the setup of the experiment. The structure under test was placed in a six-way cross vacuum chamber and mounted on an actuator, which was able to move in the vertical direction. Thus, the beam passed through the structure with an adjustable transverse offset. The chamber and the structure under test were aligned to the beam line so that the bunch could pass through the structure. A 5 nC, 14 MeV electron bunch was delivered to the vacuum chamber. Based on the simulation of the beam dynamics, the R.M.S. beam spot size was 0.5 mm, and the R.M.S.

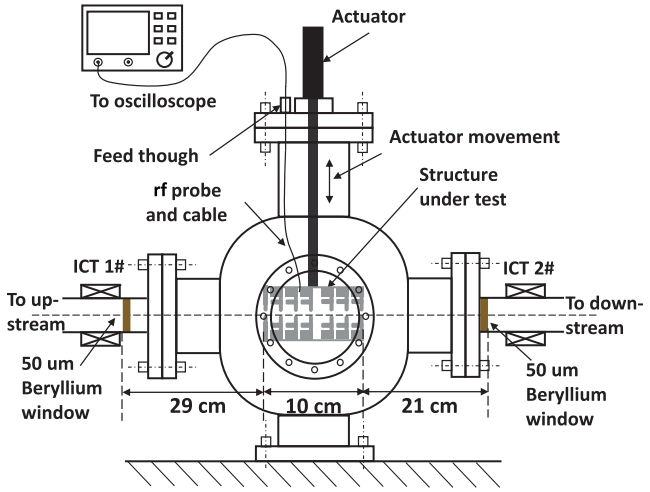

FIG. 3. Experiment setup.

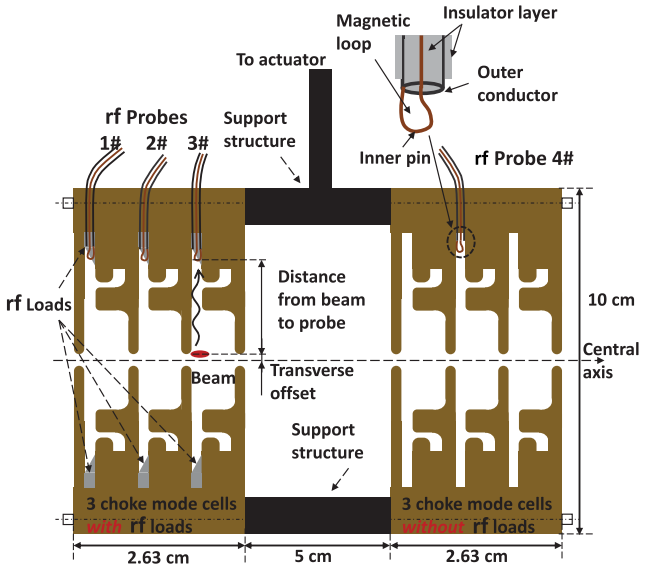

FIG. 4. Choke-mode cells in the experiment.

bunch length was about 1.5 mm. The minimum beam aperture of the structure under test was 5.5 mm, which was sufficiently large for the electron bunch to travel through.

As seen in Fig. 4, the structure under test consists of two subassembly units. Each of them contains three identical aluminum-made choke-mode cells, whose geometry is the same of the middle cell of the "CLIC-CDS-C" design [12]. One subassembly had rf loads inside each cell, and the other unit was unloaded. Such a setup allowed the observation of signals of the undamped modes. A space between two subassembly units was reserved to prevent the beam-induced signals from interfering with each other. All the disks were clamped together by long bolts.

The geometry of the rf load used for this experiment is shown in Fig. 5. The slot in the cell disks and the rf load (i.e. SiC disk) were used to place the rf probes. According

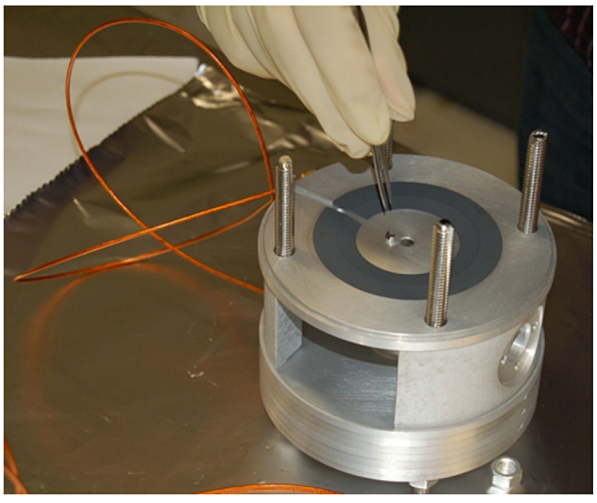

FIG. 5. Installation of the choke-mode cell disks and rf loads.

to the HFSS® [25] simulation, the reflection of this rf load was smaller than −20 dB over the frequency range from 15 GHz to 40 GHz. The −20 dB reflection caused 10% error to the Q factor, which set the error bar of this experiment.

Four Kapton insulated soft coaxial cables (30 AWG, 50 Ω) with an outer radius of 1.7 mm were used to transmit the signals [26]. A loop antenna was created at end of each cable which was placed inside the choke-mode cell to pick up the wakefield signal, as seen in Fig. 4. The other end of each Kapton cable was connected to a SMA (Sub-Miniature version A) feedthrough at the flange (see Fig. 3). A 10-m-long SMA type coaxial cable was used to transmit the rf signals from the flange to the oscilloscope, which was located outside the accelerator tunnel. The total attenuation of all the cables was approximately −20 dB at a frequency of 15 GHz. Even after the strong attenuation in the transmission system, the estimated peak signal strength was about 5 V when the bunch had a total charge of 1 nC and transverse offset of 1 mm.

In order to meet the AWA vacuum standard, two beryllium windows were installed between the vacuum chamber housing the choke mode cell assembly and the beam line to protect the clean environment of the rest of beam line, especially the cathode. The thickness of the beryllium windows was 50 μm, and this resulted in non-negligible scattering of the 14 MeV electron beam. Based on a Monte-Carlo calculation using the FLUKA code [27], approximately 70% of the electron bunch will be deflected by the beryllium window and hit the structure wall and beam pipe. The charge of electron beam which is able to reach the downstream (e.g. ICT 2#) was about 1.5 nC.

The oscilloscope used in this experiment had 2 channels, 50 GHz sampling rate and 20 GHz bandwidth. As shown in Fig. 2, the first and second dipolar modes near 17 GHz should be directly observed from the measured signal. To measure a higher frequency, a mixer was used to shift the beam-induced signal by 10 GHz; thus, the 29 GHz dipolar mode could be potentially observed. Four shifts (32 hours) of beam time were assigned to the experiment, two with the mixer and two without. At each shift, we measured the beam-induced rf signal captured by all the probes with nine different transverse offsets of the structure under test (controlled by the actuator). We measured wakefields at each transverse offset three times.

III. RESULTS AND DISCUSSION

A. Signals without mixer

Figure 6 shows one of the measured rf signals without mixer. Here, attenuators were used to reduce the signal voltage to the measurable range. As shown in the plots, the signal captured by probes #1–3 decayed quickly in time. The signal of probe #4 had a slower decay because no rf load was placed inside the choke-mode cell that hosted the #4 probe.

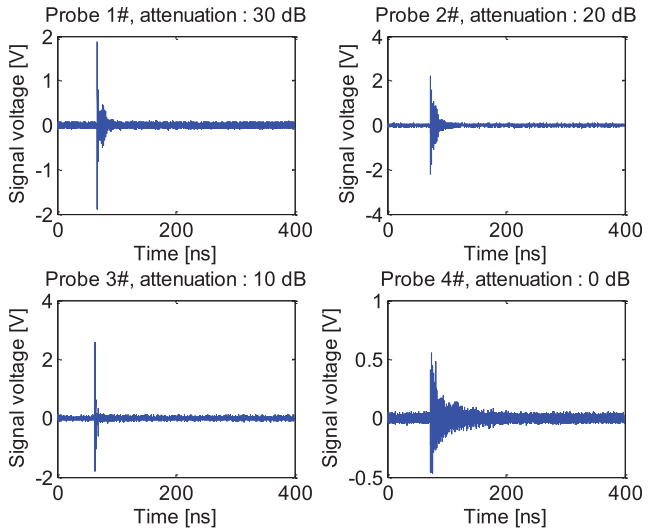

FIG. 6. Measured rf signals of all the probes without mixer.

Figure 7 shows the spectra of all the signals in Fig. 6. A high peak near 12 GHz was observed, and all the other modes were relatively insignificant in the spectra of signals from probes #1 and 2. This peak should be the fundamental accelerating mode of the *X*-band choke-mode cavities. Dipole modes near 16 and 19 GHz (shown in Fig. 2) were observed in the spectrum of probe #3. Theoretically, the fundamental accelerating mode should not be observed because it is fully reflected by the choke structure and is unable to reach the rf probes located in the outer radial line. However, given the change in the boundary condition (ideal case is the infinitely repeated cells, but in this experiment only 3 cells were used and apertures in both sides were connected to the free space, which means larger bandwidth for the mode excitation) and the error in the geometry of the

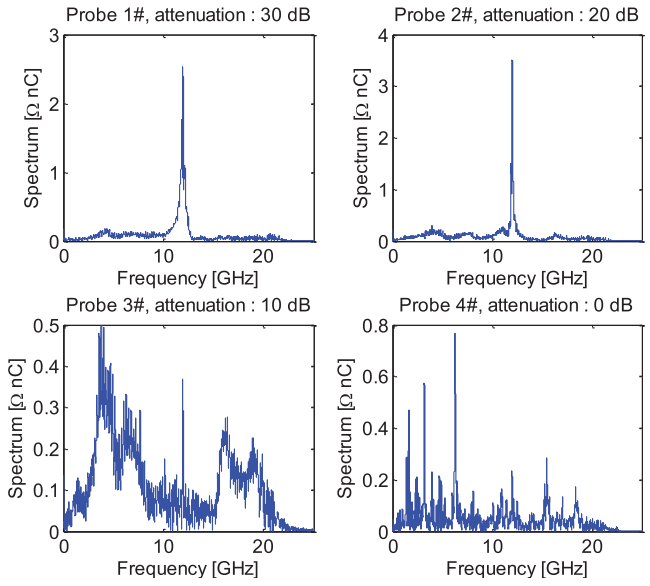

FIG. 7. Measured spectrum of all four probes without mixer.

structure due to machining (20 μm), installation and, the choke structure was unable to fully reflect this beam-excited fundamental mode. Thus, the probes could still capture signals of the fundamental mode.

As shown in Figs. 6 and 7, the signal strengths on probes #1 and #2 (without attenuator) are much greater than that of probe #3, especially for the fundamental 12 GHz mode. There are three possible explanations to the discrepancy between the signal strengths of rf probes #1, #2, and #3: (1) The coupling from excited electromagnetic field to the coaxial cable may be different for probes. This coupling is determined by the area and orientation of probe loop. However, these factors are difficult to determine off-line since installation and subsequent dismantling have the potential to change the orientation of the loop. (2) The fundamental 12 GHz mode leaked into the outer radial line has large contribution to the signal amplitude. The discrepancy between signal strength of rf probes may come from the different leakage of the 12 GHz mode in three choke-mode cells. Q-factors of the 12 GHz mode analyzed from Fig. 7 are about 120, 200, 300 and 500 for probe #1, #2, #3 and #4, respectively. Q-factors of 12 GHz mode captured by probe #1, #2, #3 (damped choke-mode cells)

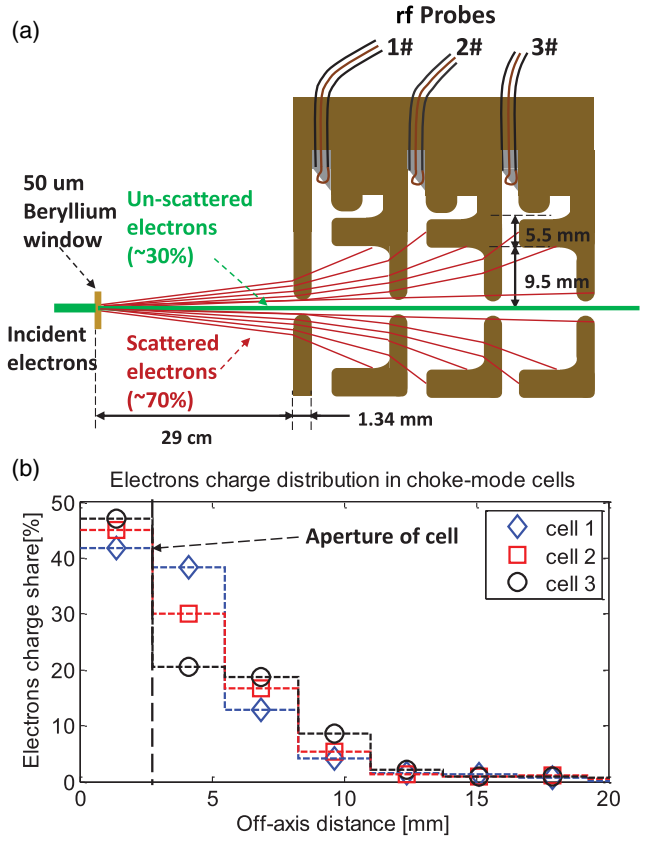

FIG. 8. (a) Schematic plot of electron beam trajectories in the structure under test; (b) Distribution of electron charge on the transverse offset in different choke-mode cells (FLUKA simulations).

are lower than that of probe #4 (undamped cell), which proves that the fundamental mode reached the outer radial line and were damped by rf loads. The discrepancy in Q-factors of 12 GHz mode of three damped cells indicates that the leakage of 12 GHz mode are different for these cells. For instance, the first choke-mode cell has lowest Q-factor of 12 GHz mode, which indicates highest leakage of 12 GHz mode in this cell. And this is the possible reason of largest signal strength in the first choke-mode cell. (3) The presence of the beryllium window may affect the electron trajectories and results in different mode excitation. According to the FLUKA simulation, the 14 MeV electron beam barely loses any kinetic energy while traversing the 50 micron thick beryllium window but multiple scattering increases the beam transverse emittance significantly which leads to 50% of the electron charge striking the wall of the first choke-mode cell disk. As penetration depth of the 14 MeV electron in the aluminum is about 15 mm, the scattered electrons crossed the disks to downstream cells but with larger scattering angle. Consequently, electrons crossed through the third choke-mode cell with larger transverse offset than through the first one. As shown in Fig. 9, the loss factor (proportional to the electrical field) of the 12 GHz mode in the cavity is smaller for the larger transverse offset. Consequently, the electron beam would have excited a lower voltage at the third cell compared to the first one. These scattered electrons also excited larger amplitude of lower order modes in the third cell since these modes (e.g., 3.8 GHz and 5.6 GHz) have higher loss factors at the large transverse offset (∼10 mm) as seen in Fig. 9.

Nevertheless the measured rf signals in probe #3 contain more useful information than the others because of the smaller signal attenuation (−10 dB) and lower amplitude of the fundamental mode. We collected all the measured signals of probe #3 and analyzed the dependency of mode strength on the transverse offset of the structure in order to discriminate the monopole and dipole modes. In the measured data set, the beam charge (measured by the ICT #1 at the upstream of the vacuum chamber) was used to normalize each signal to 5 nC. However, the charge delivered into the structure could not be directly measured. Given that the scattered electron beam could penetrate deeper than the thickness of the wall of 3 cells, the charge that crossed the third choke-mode cell was treated to be the same as the charge measured by ICT #1 (measured peak voltage of ICT #1: 80 mV, ICT #2: 37 mV).

An alignment in the time-domain, as shown in Fig. 10, was conducted for all measured signals from same probe. It was done by locating the zero-crossing time point between the first valley and first peak. This first zero-crossing time point is good for aligning because profiles of signals at here are similar to each other and the slope of the voltage is highest for more precise locating. Furthermore, the transverse offset between the beam and the tested structure affects the distance between the beam and the probe, which results in a different time delay of the excited signal (see Fig. 4 for more details). This time delay should be considered so that all signals are aligned to the time point of the beam entering the cell. This time alignment is necessary here because the relative time shift could cause a phase discrepancy of the complex spectra of all the signals, which causes difficulties in analyzing dipolar modes.

Figure 11 plots spectrum value of a dipole frequency and a monopole one in the complex plane. Each dot in this figure represents one measured signal. Dots with three different colors are plotted for different alignment schemes. The time alignment does not change the magnitude but changes the phase so different distribution of these dots are seen in the figure. The distribution of blue dots, of which signals were aligned to the time of beam entering the cell, appears most physical. The blue dots for the dipole frequency are distributed in the complex plane like a straight line, which agrees with the principle of that the spectrum value of a dipole mode is the linear function of the transverse offset. The spectrum value of a monopole frequency has no dependence on the transverse offset of beam (same magnitude and phase), so dots should be

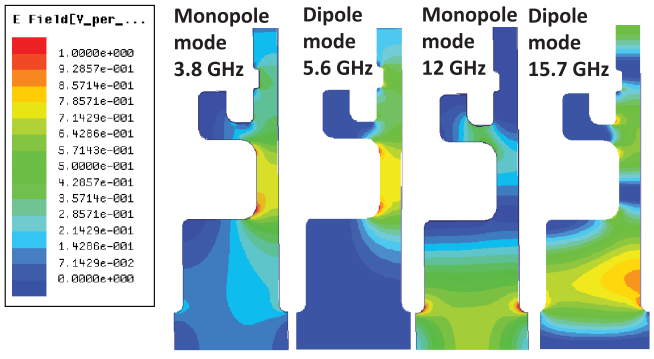

FIG. 9. Electrical field distribution of different modes in the choke-mode cell.

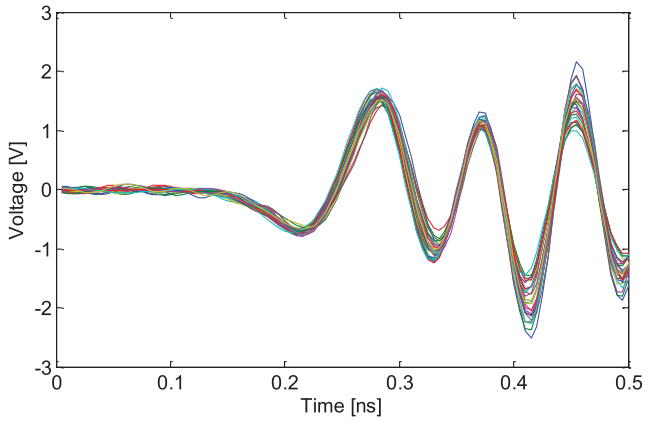

FIG. 10. Time alignment of all the signals measured by the same probe (probe 1#).

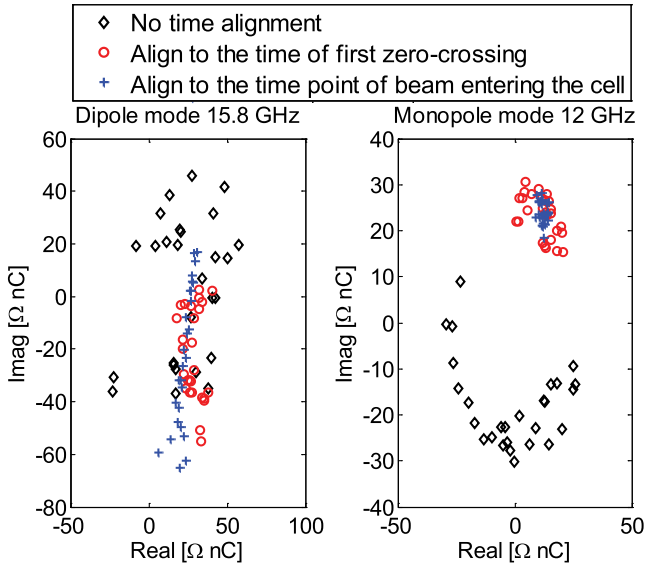

FIG. 11. Spectrum value of two frequencies (left: dipole mode; right: monopole mode) in the complex plane for different time alignment schemes.

located in the same points. As seen in the Fig. 11, blue dots are close to each other and the divergence is smaller than other colors. This discussion shows that the time alignment conducted in this work correctly adjusts the phase of each mode and helps in analyzing all signals from the same probe.

The singular value decomposition (SVD) method was used to analyze the signals of probe #3 after the time alignment. SVD could decompose signals to several mutually orthogonal modes, which was useful for finding information with a certain pattern and also helped in separating the noise from the signal. We formed all the measured data from probe #3 into a matrix. The SVD operation in this matrix is shown in the equation below, where $\boldsymbol{X}_i$ is a column eigenvector, $\boldsymbol{Y}_i{}^{\mathrm{T}}$ is a row eigenvector, and β_i is the eigenvalue of the ith SVD mode. Each SVD mode is orthogonal to all the other modes, which means that $\boldsymbol{X}_i{}^{\mathrm{T}}\boldsymbol{X}_j = \boldsymbol{Y}_i{}^{\mathrm{T}}\boldsymbol{Y}_j = 0$ when $i \neq j$.

$$\boldsymbol{D} = \sum_i \beta_i \boldsymbol{X}_i \boldsymbol{Y}_i{}^{\mathrm{T}} \tag{1}$$

The eigenvectors $\boldsymbol{X}_i$ and $\boldsymbol{Y}_i{}^{\mathrm{T}}$ here manifest signal voltage distributions on two different dimensions for one SVD mode. For the measured data set matrix $\boldsymbol{D}$, the row number refers to different sample times, and the column number refers to all the measured signal data at different actuator offsets. Thus, $\boldsymbol{X}_i$ represents the signal voltage as a function of time, and $\boldsymbol{Y}_i{}^{\mathrm{T}}$ represents amplitudes of the signal pattern $\boldsymbol{X}_i$ in all the measured signals. Figure 12(a) shows the plot of the eigenvector $\boldsymbol{Y}_i{}^{\mathrm{T}}$ of the first and second SVD modes versus the actuator offsets. From the plot, the first SVD mode is similar to the signal of monopole modes, and the

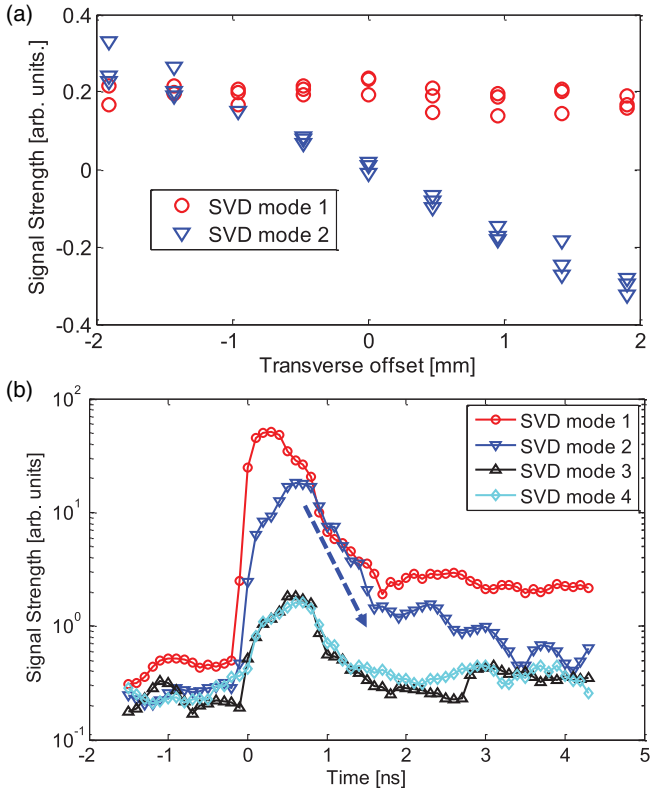

FIG. 12. Signal strength of each SVD mode versus (a) transverse offset; (b) time.

second SVD mode to dipole modes. Figure 12(b) shows the signal strength of each SVD mode versus time. Here, the signal strength at a given point in time is calculated by the mean amplitude over the nearby time range ($+/-0.2$ ns). As seen in Fig. 12(b), all the SVD modes start to rise when the electron beam arrives (at zero time shown in the plot) and then decays. The first and second SVD modes have much larger amplitude than all the others. The amplitudes of the third and fourth modes are about 10 times higher than the noise level (about 0.2–0.3 arb. Units, based on the amplitude before the beam enters). The signal to noise ratios of third and fourth modes are not sufficient for analyzing HOMs.

Figure 13(a) shows the spectra of the first and second SVD modes. The spectrum of the second SVD mode shows clearly two dipole peaks at 15.8 and 18.9 GHz. The width at half maximum of each peak is nearly 1.1 GHz; the estimated Q factors of the two modes are 14 and 18. These findings are also verified in Fig. 12(b), which shows that the signal strength of the second SVD mode decays by a factor of nine from 0.9 ns to 1.6 ns. In the simulation results shown in Fig. 2, the frequencies of the two dipole peaks are 15.8 and 18.9 GHz, and the Q factors are 13 and 15, respectively. Good agreement between the measured data and simulated data is demonstrated in the analyzed results. Figure 13(b) shows another way of using a linear fit to identify the dipole modes. It was performed in this way:

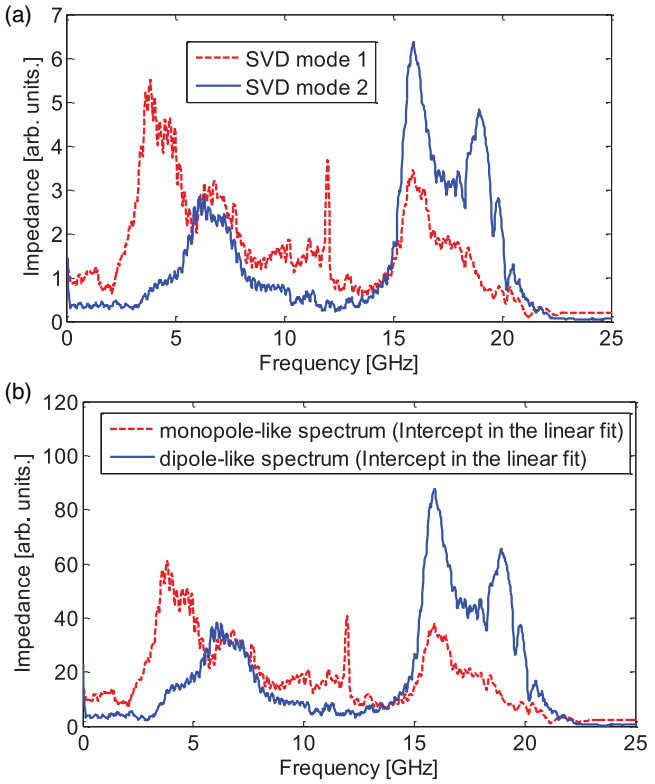

FIG. 13. (a) Spectrum of the first and second SVD modes and (b) linear fit of the spectrum of all the signals on the transverse offset.

the complex number spectrum of each signal is $H_{i,j}$, where the subscript i is the index of frequency point and j is the index of the repeated measured data (with different transverse offset). The strength of dipole mode component is proportional to the transverse offset Δy_j and the strength of monopole mode component has no dependence on Δy_j. Thus the theoretical value of $H_{i,j}$ is expressed as below:

$$H_{i,j} = d_i \Delta y_j + m_i \tag{2}$$

Where d_i and m_i are the strength of dipole and monopole mode component, respectively. Here for each frequency point f_i, the slope d_i and intercept m_i are able to be solved numerically by linear fit of spectrum value of all signals $H_{i,j=1..N}$ on the transverse offset Δy_j. Plots of d_i and m_i versus frequency f_i are the dipole-like and monopole-like spectrum, as shown in Fig. 13 (b). Results analyzed from the linear fit method are similar as those of the SVD method.

In the spectrum of the second SVD mode, a small peak near 21 GHz was observed. However as shown in Fig. 2, no dipole peak was near this frequency. According to the Nyquist theorem, the 21 GHz peak could possibly be the aliasing frequency of a 29 GHz signal (sampling frequency: 50 GHz), which was close to the 28 GHz dipole mode shown in Fig. 2. If this is true, the 29 GHz dipole mode was measured at an estimated Q factor of 20. Lower-order modes (3–5 GHz) were also appreciable in both the first and the second SVD modes, as the reason was explained in Fig. 8 and Fig. 9.

The signals of the other probes could be analyzed in the same way as those for probe #3. Figure 14(a) shows the spectra of the first and second SVD modes from the signals measured by probe #1. The spectra of both the SVD modes for probe #1 were dominated by the working frequency. However, two dipole modes near 16 and 19 GHz were still observed. Given the stronger attenuator (−30 dB) used for the probe #1, the amplitude of the dipole modes shown in Fig. 14(a) were much lower than those of probe #3.

Figure 14(b) shows spectrum of the signals from probe #4. All the peaks in the impedance of the undamped choke mode cell (see Fig. 2) are also observed in Fig. 14(b). Many unidentified modes are also shown in the spectrum. However, given the lack of experimental evidence, we could not determine whether these unidentified peaks are physical modes or not.

B. Signals with mixer

The measured signals with frequency mixer (mixed with 10 GHz LO) could not be aligned in the time domain because the waveforms of all the signals were no longer similar to one another after the mixer changed the beat of all

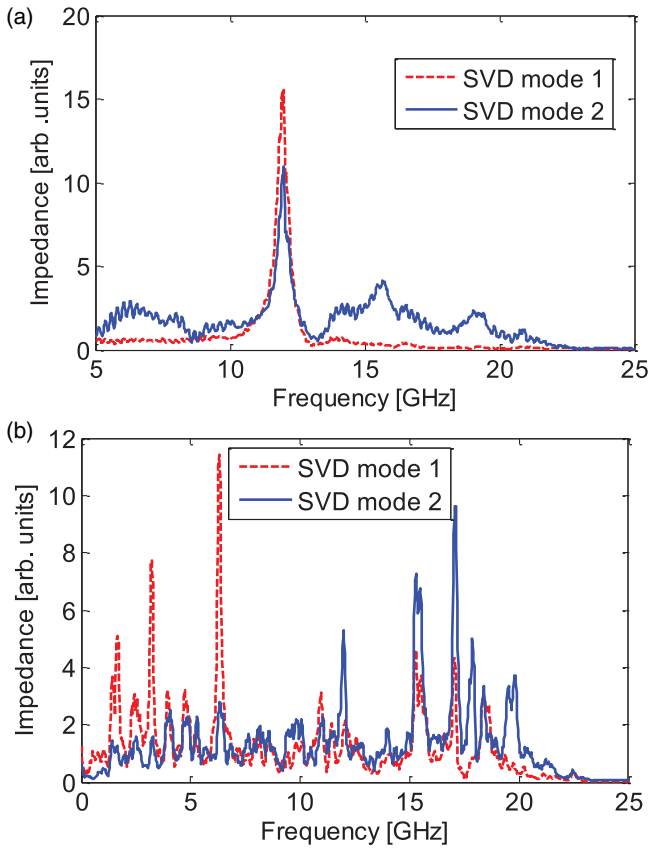

FIG. 14. Spectrum of the first and second SVD modes of probes (a) #1 and (b) #4.

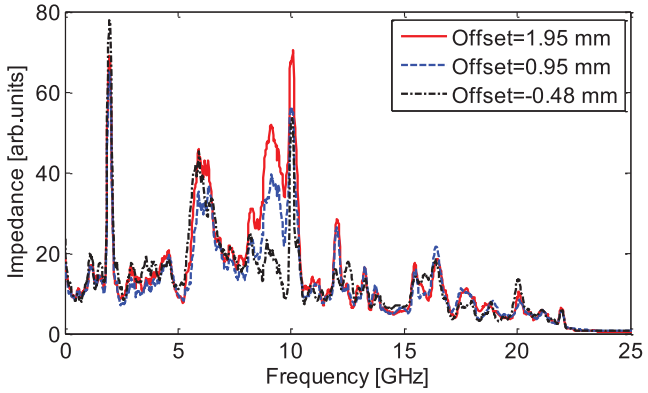

FIG. 15. Spectrum of the measured signals with mixer.

the signals. Consequently, the SVD method or linear fit was no longer applicable here. The dipole modes could be identified only by qualitatively comparing the spectra of the signals measured by probe #3 with different transverse offsets.

Figure 15 shows the spectra of the signals in three different offsets. As seen in the spectrum, the peak near 2 GHz represents the fundamental mode. The two peaks near 6 and 9 GHz are the dipole modes near 16 and 19 GHz, respectively. The 10 GHz peak is the original mixer frequency. A small peak near 18 GHz may represent the dipole modes near 28 GHz. However, given the additional attenuation in the mixer (−15 dB), the signals recorded by the oscilloscope were weak (peak voltage: 0.5 V, noise voltage: 0.05 V). The precision is insufficient to identify the peaks with a frequency higher than 10 GHz.

IV CONCLUSION

The beam-induced wakefield in an *X*-band choke-mode structure was obtained. Based on the analysis the following conclusions were drawn: 1. A fundamental accelerating mode (12 GHz) and two major dipole modes (16 GHz and 19 GHz) are observed in the measurements. Good agreement between the measured data and the simulated data is demonstrated, particularly in terms of the frequency and Q factor of these two dipole modes. The two modes observed in the experiment are heavily damped ($Q \sim 15$) and the 3 GHz difference between them leads them to cancel each other out at the time of the next bunch (0.5 ns), which verifies the wakefield suppression of the new choke-mode geometry design. 2. Electrons scattered by the beryllium window penetrate the cell disks with a large transverse offset. These electrons excite strong signals of lower-order modes, which are not within the scope of this experiment. Future similar experiments should consider using a collimator to absorb the scattered beam in case the beryllium window is needed. 3. This experiment employs the SVD method after aligning all the measured signals in the time-domain and demonstrates its advantages in dissociating noise and identifying the mode. 4. The 28 GHz dipole was observed in the experiment but at very low amplitude. Given the strong attenuation in the long and sophisticated signal transport system, the modes with a frequency higher than 20 GHz are difficult to identify with or without a mixer.

ACKNOWLEDGMENTS

The authors thank Chuanjing Wang for his invaluable assistance in manufacturing all the disks. The authors also thank Xiaowei Wu, Yawei Yang, Alexej Grudiev, and Walter Wuensch for their helpful discussions. This work is supported by DOE under contract W-31-109-ENG-38 and the National Natural Science Foundation of China (NSFC) (Grant Nos. 11135004 and 11375098).

[1] W. K. H. Panofsky and M. Bander, Asymptotic theory of beam break- up in linear accelerators, Rev. Sci. Instrum. **39**, 206 (1968).

[2] R. Helm and G. Loew, in *Linear Accelerators*, edited by P. M. Lapostolle and A. L. Septier (North-Holland, Amsterdam, 1970), Ch. B.1.4, p. 173.

[3] K. L. F. Bane and R. L. Gluckstern, Report No. SLAC PUB-5783, 1992.

[4] H. Deruyter *et al.*, Damped and detuned accelerator structures, *Proceedings of the 1990 Lin. Acc. Conf., Albuquerque, NM* (1990), p. 132; also in SLAC PUB-5322.

[5] J. W. Wang *et al.*, Wakefield measurements of SLAC linac structures at the Argonne AATF, in *Proceedings of the IEEE 1991 Particle Accelerator Conference (APS Beams Physics)* (IEEE, Piscataway, NJ, 1991), p. 3219; also in, Report No. SLAC-PUB-5498, 1991.

[6] I. Syratchev, Report No. CERN-AB-2005-086-CLIC Note 643, 2005.

[7] H. H. Braun *et al.*, Report No. CERN-CLIC-Note 364, 1998.

[8] T. Shintake, The choke mode cavity, Jpn. J. Appl. Phys. **31**, L1567 (1992).

[9] T. Shintake, High power test of HOM-free choke-mode damped accelerating structure, in *Proceeding of the 17th Linear Accelerator Conference, LINAC-1994, Tsukuba, Japan* (JACoW, Tsukuba, Japan, 1994), MO-91.

[10] T. Shintake *et al.*, The first wakefield test on the C-band choke-mode accelerating structure, in *Proceedings of the 18th Particle Accelerator Conference, New York, 1999* (IEEE, New York, 1999), FRA14.

[11] J. Shi *et al.*, Design of a Choke-mode Damped Accelerating Structure for CLIC Main Linac, in *Proceedings of the 2nd International Particle Accelerator Conference, IPAC-2011, San Sebastián, Spain* (EPS-AG, Spain, 2011), MOPC021.

[12] H. Zha, J. Shi, H. Chen, A. Grudiev, W. Wuensch, C. Tang, and W. Huang, Choke-mode damped structure design for the Compact Linear Collider main linac, Phys. Rev. ST Accel. Beams **15**, 122003 (2012).

[13] CLIC Conceptual Design Report (CDR), 2012, http://project-clic-cdr.web.cern.ch/project-CLIC-CDR/CDR_Volume1.pdf.

[14] A. Grudiev *et al.*, Design of the CLIC main linac accelerating structure for CLIC Conceptual Design Report, in *Proceedings of the 25th International Linear Accelerator*

Conference, LINAC-2010, Tsukuba, Japan (KEK, Tsukuba, Japan, 2010).
[15] V. F. Khan. Ph.D. thesis, University of Manchester, 2010.
[16] AWA facility in Argonne National Laboratory, http://www.hep.anl.gov/awa/index.html.
[17] C. Jing *et al.*, Observation of wakefields in a beam-driven photonic band gap accelerating structure, Phys. Rev. ST Accel. Beams **12**, 121302 (2009).
[18] R. A. Marsh, M. A. Shapiro, R. J. Temkin, E. I. Smirnova, and J. F. DeFord, Measurement of wakefields in a 17 GHz photonic band gap accelerator structure, Nucl. Instrum. Methods Phys. Res., Sect. A **618**, 16 (2010).
[19] E. I. Simakov, S. A. Arsenyev, C. E. Buechler, R. L. Edwards, W. P. Romero, M. Conde, G. Ha, J. G. Power, E. E. Wisniewski, and C. Jing, Observation of Wakefield Suppression in a Photonic-Band-Gap Accelerator Structure, Phys. Rev. Lett. **116**, 064801 (2016).
[20] R. M. Jones, Wakefield suppression in high gradient linacs for lepton linear colliders, Phys. Rev. ST Accel. Beams **12**, 104801 (2009).
[21] C. Adolphsen, K. Bane, T. Higo, K. Kubo, R. Miller, R. Ruth, K. Thompson, and J. Wang, Measurement of Wake-Field Suppression in a Detuned *X*-Band Accelerator Structure, Phys. Rev. Lett. **74**, 2475 (1995).
[22] I. Wilson *et al.*, An ASSET test of the CLIC accelerating structure, in *Proceedings of the European Particle Accelerator Conference, Vienna, 2000* (EPS, Geneva, 2000), THP2A18.
[23] H. Zha, A. Latina, A. Grudiev, G. De Michele, A. Solodko, W. Wuensch, D. Schulte, E. Adli, N. Lipkowitz, and G. S. Yocky, Beam-based measurements of long range transverse wakefields in the Compact Linear Collider main-linac accelerating structure. Phys. Rev. Accel. Beams **19**, 011001 (2016).
[24] FACET facility in SLAC National Laboratory, http://portal.slac.stanford.edu/sites/ard_public/facet/Pages/default.aspx.
[25] Ansoft HFSS, http://www.ansoft.com.
[26] Accu-Glass Products, Inc. https://accuglassproducts.com/product.php?productid=17333.
[27] Fluka code, http://www.fluka.org/fluka.php.